Quantum and Classical Lyapunov Exponents in Atom-Field Interaction Systems

Jorge Chávez-Carlos,[1] B. López-del-Carpio,[1] Miguel A. Bastarrachea-Magnani,[2] Pavel Stránský,[3] Sergio Lerma-Hernández,[4] Lea F. Santos,[5] and Jorge G. Hirsch[1]

[1]*Instituto de Ciencias Nucleares, Universidad Nacional Autónoma de México, Apdo. Postal 70-543, C.P. 04510 Cd. Mx., México*

[2]*Physikalisches Institut, Albert-Ludwigs-Universitat Freiburg, Hermann-Herder-Str. 3, Freiburg D-79104, Germany*

[3]*Faculty of Mathematics and Physics, Charles University, V Holešovičkách 2, Prague 180 00, Czech Republic*

[4]*Facultad de Física, Universidad Veracruzana, Circuito Aguirre Beltrán s/n, Xalapa, Veracruz 91000, Mexico*

[5]*Department of Physics, Yeshiva University, New York, New York 10016, USA*

(Received 27 July 2018; revised manuscript received 19 September 2018; published 15 January 2019)

The exponential growth of the out-of-time-ordered correlator (OTOC) has been proposed as a quantum signature of classical chaos. The growth rate is expected to coincide with the classical Lyapunov exponent. This quantum-classical correspondence has been corroborated for the kicked rotor and the stadium billiard, which are one-body chaotic systems. The conjecture has not yet been validated for realistic systems with interactions. We make progress in this direction by studying the OTOC in the Dicke model, where two-level atoms cooperatively interact with a quantized radiation field. For parameters where the model is chaotic in the classical limit, the OTOC increases exponentially in time with a rate that closely follows the classical Lyapunov exponent.

DOI: 10.1103/PhysRevLett.122.024101

Quantum chaos tries to bridge quantum and classical mechanics. The search for quantum signatures of classical chaos has ranged from level statistics [1,2] and the structure of the eigenstates [3,4] to the exponential increase of complexity [5,6] and the exponential decay of the overlap of two wave packets [7–10]. Recently, the pursuit of exponential instabilities in the quantum domain has been revived by the conjecture of a bound on the rate growth of the out-of-time-ordered correlator (OTOC) [11,12]. First introduced in the context of superconductivity [13], the OTOC is now presented as a measure of quantum chaos, with its growth rate being associated with the classical Lyapunov exponent. The OTOC is not only a theoretical quantity, but has also been measured experimentally via nuclear magnetic resonance techniques [14–17].

The correspondence between the OTOC growth rate and the classical Lyapunov exponent has been explicitly shown in two cases of one-body chaotic systems, the kicked rotor [18] and, after a first unsuccessful attempt [19], the stadium billiard [20]. It was also achieved for chaotic maps [21]. For interacting many-body systems, while exponential behaviors for the OTOC have been found for the Sachdev-Ye-Kitaev model [11,22] and for the Bose-Hubbard model [23,24], a direct demonstration of the quantum-classical correspondence has not yet been made. Studies in this direction include [6,25–29] and [30].

Here, we investigate the OTOC for the Dicke model [31,32]. Comparing with one-body systems, the model is a step up toward an explicit quantum-classical correspondence for interacting many-body systems, since it contains N atoms interacting with a quantized field.

The Dicke model was originally proposed to explain the collective phenomenon of super-radiance: the field mediates interatomic interactions, which causes the atoms to act collectively [31,33]. Super-radiance has been experimentally studied with ultracold atoms in optical cavities [34–39]. The model has also found applications beyond super-radiance in various different fields. It has been employed, for instance, in studies of ground-state and excited-state quantum phase transitions [33,40–44], entanglement creation [45], nonequilibrium dynamics [46–49], quantum chaos [50–53], and monodromy [54,55]. Recently, the model has received revived attention due to new experiments with ion traps [56,57] and the analysis of the OTOC [58,59].

In the classical limit, the Dicke model presents regular and chaotic regions depending on the Hamiltonian parameters and excitation energies [53]. This allows us to benchmark the OTOC growth against the presence and absence of chaos. The results in the chaotic region display three different temporal behaviors: a sinusoidal evolution at short times, followed by an exponential growth, that holds up to the saturation of the dynamics. Our approach, based on the use of an efficient basis for the convergence of the eigenstates, enables the treatment of systems that are large enough to reveal the exponential part of the dynamics. We find that the exponential growth rate is in close agreement with the classical Lyapunov exponent.

Quantum and classical Hamiltonian.—The Dicke model has N two-level atoms of level spacing ω_0 coupled with a single mode of a quantized radiation field of frequency ω. The Hamiltonian is given by

$$\hat{H}_D = \frac{\omega}{2}(\hat{p}^2+\hat{q}^2) + \omega_0 \hat{J}_z + 2\frac{\gamma}{\sqrt{N/2}}\hat{J}_x\hat{q} - \frac{\omega}{2}, \quad (1)$$

where $\hbar = 1$; $\hat{q} = (\hat{a}^\dagger + \hat{a})/\sqrt{2}$ and $\hat{p} = i(\hat{a}^\dagger - \hat{a})/\sqrt{2}$ are the quadratures of the bosonic field and $\hat{a}(\hat{a}^\dagger)$ is the annihilation (creation) operator; γ is the atom-field interaction strength; and the collective atomic pseudo-spin operators, $\hat{J}_{x,y,z} = (1/2)\sum_{n=1}^{N}\sigma_{x,y,z}^{(n)}$, are the sums of the Pauli matrices for each atom n. The eigenvalue of the total spin operator $\hat{J}^2 = \hat{J}_x^2 + \hat{J}_y^2 + \hat{J}_z^2$ is $j(j+1)$. The critical point $\gamma_c = \sqrt{N/(2j)}\sqrt{\omega\omega_0}/2$ marks the transition from a normal phase ($\gamma < \gamma_c$) to a super-radiant phase ($\gamma > \gamma_c$). We set $\omega = \omega_0 = 1$ in the illustrations below and work with the symmetric atomic subspace ($j = N/2$), where the ground state lies. The model has two degrees of freedom.

The classical Hamiltonian is built by employing Bloch coherent states and Glauber coherent states [53,60,61]. The first are given by $|z\rangle = (1+|z|^2)^{-j}e^{z\hat{J}_+}|j,-j\rangle$, where $z \in \mathbb{C}$ and $|j,-j\rangle$ is the ground state for the atoms. The Glauber coherent states are $|\alpha\rangle = e^{-|\alpha|^2/2}e^{\alpha\hat{a}^\dagger}|0\rangle$, where $\alpha \in \mathbb{C}$ and $|0\rangle$ is the photon vacuum. The canonical variables (p,q) and (j_z,ϕ) are given in terms of the coherent state parameters $\alpha = \sqrt{(j/2)}(q+ip)$ and $z = \sqrt{[(1+j_z)/(1-j_z)]}e^{-i\phi}$, respectively. Deriving the classical Hamiltonian is basically equivalent to replacing the operators with the canonical variables (q,p) and (j_z,ϕ) as $\hat{q} \to \sqrt{j}q$, $\hat{p} \to \sqrt{j}p$, $\hat{J}_z \to jj_z$, $\hat{J}_x \to j\sqrt{1-j_z^2}\cos\phi$. It reads

$$H_D^{\mathrm{cl}} = j\frac{\omega}{2}(p^2+q^2) + j\omega_0 j_z + 2j\gamma\sqrt{1-j_z^2}q\cos\phi. \quad (2)$$

Since the classical limit is reached for $j \to \infty$, the effective Planck constant is $\hbar_{\mathrm{eff}} = 1/j$.

We denote the energy per particle as $\epsilon = H_D^{\mathrm{cl}}/j$, which is independent of j. Since the number of bosons in the field is unlimited, the range of values of ϵ is only limited from below. The ground-state energy is given by $\epsilon_0(\gamma) = -\omega_0$ for $\gamma \le \gamma_c$ and by $\epsilon_0(\gamma) = -(\omega_0/2)[(\gamma_c^2/\gamma^2) + (\gamma^2/\gamma_c^2)]$ for $\gamma > \gamma_c$.

With the classical Hamiltonian, we obtain a map of the degree of chaoticity of the system as a function of the energy ϵ and the interaction strength γ, as shown in Fig. 1. The task of drawing the map is quite demanding. For each value of ϵ and γ, we consider a large sample of initial conditions distributed homogeneously in the energy shell. The Lyapunov exponent λ_{cl} is evaluated for each initial condition solving the dynamical equations and the fundamental matrix simultaneously [53]. If $\lambda_{\mathrm{cl}} > 0$, the initial condition is chaotic and for $\lambda_{\mathrm{cl}} = 0$, the initial condition is regular. The percentage of chaos is defined as the ratio of the number of chaotic initial conditions over the total number of initial conditions in the sample. This percentage is shown in Fig. 1 with a color gradient: dark indicates

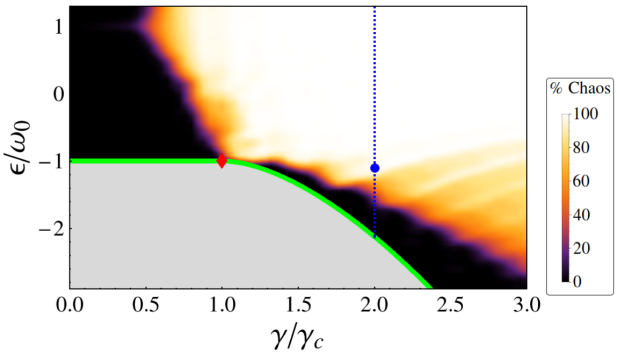

FIG. 1. Percentage of chaos over energy shells as a function of energy and coupling strength. The thick (green) solid line follows the ground-state energy and the diamond marks the critical point. The (blue) vertical dotted line indicates the coupling $\gamma = 2\gamma_c$ and the circle marks the energy chosen for the studies below.

that most initial conditions are regular and light indicates that most are chaotic. (Notice that one should look only at the results above the thick solid line that marks the ground state.) Regularity predominates for $\gamma/\gamma_c < 0.6$. For $\gamma/\gamma_c > 0.6$, most regular trajectories have low energies, while large energies are associated with chaos. This map guides our analysis of the OTOC below.

Method.—The OTOC quantifies the degree of noncommutativity in time between two Hermitian operators with small or null commutator at time $t = 0$. In terms of position and momentum, it is written as

$$C_n^{qp}(t) = -\langle\Psi_n|[q(t),p(0)]^2|\Psi_n\rangle, \quad (3)$$

where $|\Psi_n\rangle$ and E_n are the eigenstates and eigenvalues of $\hat{H}_D$. In Ref. [19], $C_n^{qp}(t)$ is called microcanonical OTOC. We refer to the exponential growth rate of the OTOC as Λ_Q. In the semiclassical limit, substituting the commutator by the Poisson bracket, one gets for a classically chaotic system, $\{q(t),p(0)\} = \partial q(t)/\partial q(0) \sim e^{\lambda_{\mathrm{cl}}t}$, where λ_{cl} is the classical Lyapunov exponent. This suggests the connection between Λ_Q and λ_{cl}, and justifies referring to Λ_Q as the quantum Lyapunov exponent.

Using the temporal evolution of the operator $\hat{q}(t) = e^{i\hat{H}t}\hat{q}e^{-i\hat{H}t}$, Eq. (3) can be expressed as [19]

$$C_n^{qp}(t) = \sum_l b_{nl}(t)b_{nl}^*(t), \quad (4)$$

where the matrix elements

$$\begin{aligned} b_{nl}(t) &= -i\langle\Psi_n|[\hat{q}(t),\hat{p}(0)]|\Psi_l\rangle \\ &= -i\sum_k (e^{i\Omega_{nk}t}q_{nk}p_{kl} - e^{i\Omega_{kl}t}p_{nk}q_{kl}), \end{aligned}$$

with $q_{nk} = \langle\Psi_n|\hat{q}|\Psi_k\rangle$, $p_{nk} = \langle\Psi_n|\hat{p}|\Psi_k\rangle$, and $\Omega_{nk} = E_n - E_k$. Since the Dicke Hamiltonian is of the form $\hat{H}_D = \omega\hat{p}^2/2 + V(\hat{q})$ and $[\hat{H}_D,\hat{q}] = -i\omega\hat{p}$,

$$b_{nl}(t) = \frac{1}{\omega}\sum_k q_{nk}q_{kl}(\Omega_{kl}e^{i\Omega_{nk}t} - \Omega_{nk}e^{i\Omega_{kl}t}), \qquad (5)$$

which simplifies the calculations. The OTOC is obtained by evaluating numerically only the matrix elements of $\hat{q}$ in the energy eigenbasis. For this, instead of employing the usual photon number (Fock) basis, we resort to an efficient basis that guarantees convergence of the eigenvalues and wave functions for a broad part of the spectrum (see [62]).

Quantum Lyapunov exponent.— In this Letter, we concentrate our analysis on chaotic eigenstates. They are chosen along the vertical line in Fig. 1, where the coupling parameter is strong, $\gamma = 2\gamma_c$. This line exhibits regular and chaotic regions. From the ground state $\epsilon_0 = -2.125$ to $\epsilon \approx -1.6$, the dynamics is regular. From $\epsilon \approx -1.6$ to $\epsilon \approx -1.2$, regular and chaotic trajectories coexist. For larger energies, $\epsilon > -1.2$, chaos covers almost the whole energy shell. We select a group of fifty-one eigenstates in the chaotic energy region with $E_n/(j\omega_0) \in (-1.11, -1.09)$. They are indicated with a circle in Fig. 1.

In Fig. 2(a), we show that even for a single representative eigenstate, the behavior of the OTOC is clearly exponential from $t \gtrsim \pi/\omega_0$ up to the saturation of the dynamics. The growth rate $\Lambda_Q = 0.139$ is obtained by fitting the curve with a straight line indicated with stars in the figure.

The exponential behavior is robust with respect to two different probes.

(i) It holds when we use the commutator for the operator $\hat{q}$ at different times, $C_n^{qq}(t) = -\langle\Psi_n|[q(t), q(0)]^2|\Psi_n\rangle$, as also shown in Fig. 2(a). The associated fit, indicated with circles, provides $\Lambda'_Q = 0.139$. Both exponential fits lead, within the numerical uncertainty, to the same quantum Lyapunov exponents.

(ii) The exponential growth rates are very similar for the fifty-one different states selected in the chaotic region.

The log-log plot in Fig. 2(b) makes evident the appearance of different behaviors at different time scales. For $t < \pi/\omega_0$, the dynamics of $C_n^{qp}(t)$ [similarly for $C_n^{qq}(t)$] is controlled by the diagonal matrix elements in Eq. (5), $b_{nn}(t) = (2/\omega)\sum_k q_{kn}^2\Omega_{kn}\cos(\Omega_{kn}t)$, with few states contributing significantly to the sum, all with energy differences $\Omega \approx 1.0$. The short-time evolution is therefore approximately described by the square of a cosine function [sine for $C_n^{qq}(t)$]. The two sinusoidal curves are shown with dotted lines in the inset of Fig. 2(b).

At long times, the quantum dynamics saturates to the infinite-time average,

$$\overline{C_n^{pq}} = \frac{1}{\omega^2}\sum_{k,l} q_{nk}^2 q_{kl}^2(\Omega_{kl}^2 + \Omega_{nk}^2), \qquad (6)$$

which is obtained from Eqs. (3) and (5) using that $\overline{\exp[i(\Omega_{ij} - \Omega_{kl})t} = 0$ for $\Omega_{ij} \neq \Omega_{kl}$. $\overline{C_n^{pq}}$ and $\overline{C_n^{qq}}$ are shown in Fig. 2(b) with dotted lines. These averages are related with the square of the size of the available phase space [19]. For the Dicke Hamiltonian, it scales with j^2 and with the number of bosons in the system, which grows with the excitation energy.

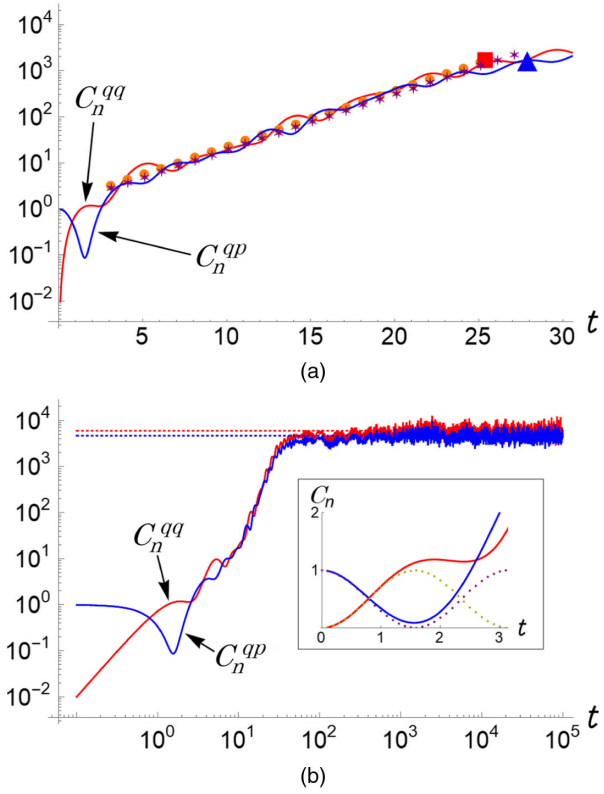

FIG. 2. Panel (a): Exponential growth of the OTOC for an eigenstate with $E_n/(j\omega_0) \approx -1.1$; numerical results (solid line), fit for $C_n^{qp}(t)$ (stars) and for $C_n qq(t)$ (circles); saturation times (square and triangle). Panel (b): Log-log plot for the evolution of the OTOC and saturation value (dotted lines). Inset: short time behavior compared with $\sin^2(t)$ and $\cos^2(t)$ (dotted lines). We use $j = 100$, $n = 1625$.

After the exponential growth, the OTOC fluctuates around its asymptotic value, as seen in Fig. 2(b), with a standard deviation σ. We define the saturation time t_S as the time when the OTOC reaches for the first time the value $\overline{C_n^{pq}} - \sigma$. The values of t_S for $C_n^{qp}(t)$ and $C_n^{qq}(t)$ are marked in Fig. 2(a) with a triangle and a square, respectively. The saturation time marks the point beyond which quantum effects are strong and the quantum-classical correspondence no longer holds, therefore the association between t_S and the Ehrenfest time. The saturation of the dynamics for finite quantum systems is in contrast to what one finds for classical systems, where the spectrum is continuous. As j increases and the system approaches the classical limit, $\overline{C_n^{pq}}$ grows and t_S increases with it.

Quantum-classical correspondence.— In a fully chaotic system, there is one classical Lyapunov exponent associated with the whole energy shell. Numerically, however, the Lyapunov exponents are computed for finite times, so they depend on the initial conditions. We evaluated the

time average of the exponents for each trajectory up to 10000 units of time, which is enough to have stable results. The trajectories for several initial conditions are depicted in Fig. 3(a). This figure shows the Poincaré surfaces of section projected on the plane (q, p) for $\phi = 0$ and energy $-1.1\omega_0$. In addition to chaotic trajectories, one identifies also regular trajectories. These islands of stability are clearly visible in Fig. 3(b) as small black regions. This bottom panel is a classical map of chaos for the same energy and plane of Fig. 3(a). The color code represents the values of the finite-time Lyapunov exponents obtained for each initial point in the phase space.

We consider thousands of initial conditions, from which a large number N_{ch} is chaotic. To obtain a single value for the Lyapunov exponent for the chaotic region of the energy shell, we average over those initial conditions that give rise to classical chaotic trajectories and discard those with zero exponents. We then have

$$\tilde{\lambda}_{\langle \ln \rangle} = \frac{1}{N_{\rm ch}} \sum_{k=1}^{N_{\rm ch}} \lambda_k = \lim_{t\to\infty} \frac{1}{t} \frac{1}{N_{\rm ch}} \sum_{k=1}^{N_{\rm ch}} \ln(e^{\lambda_k t}). \tag{7}$$

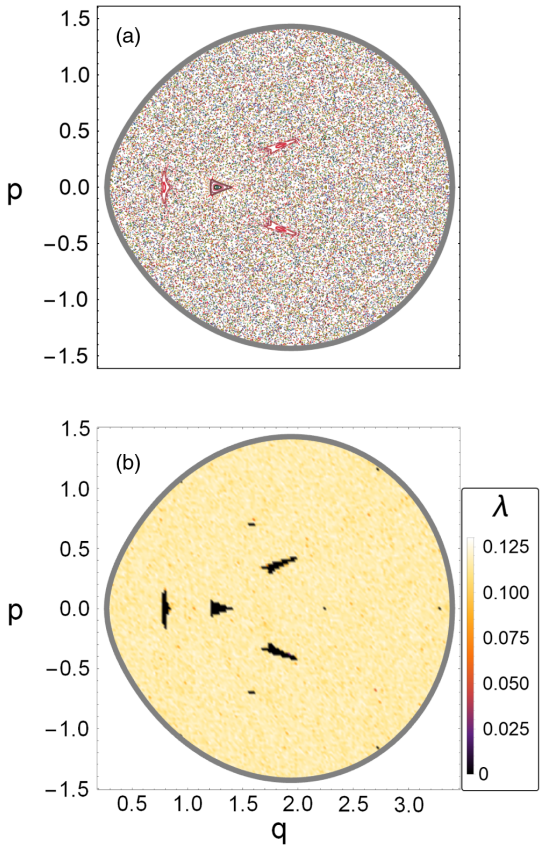

FIG. 3. Panel (a): Poincaré surfaces of section projected on the plane (q, p) for $\phi = 0$ and energy $-1.1\omega_0$ for various initial conditions. Panel (b): map of chaos over the same Poincaré surface in terms of the finite-time classical Lyapunov exponents. These exponents are evaluated for each trajectory up to 10000 units of time, which is enough to have stable results.

The purpose of writing the last term above is to emphasize that the classical Lyapunov exponent $\tilde{\lambda}_{\langle \ln \rangle}$ is the average of logarithms. We can, however, compute also the logarithm of the average,

$$\tilde{\lambda}_{\ln\langle . \rangle} = \lim_{t\to\infty} \frac{1}{t} \ln \left(\frac{1}{N_{\rm ch}} \sum_{k}^{N_{\rm ch}} e^{\lambda_k t} \right)$$
$$= \lambda_{\max} + \lim_{t\to\infty} \frac{1}{t} \ln \left(\frac{1}{N_{\rm ch}} \sum_{k} e^{(\lambda_k - \lambda_{\max})t} \right) \to \lambda_{\max}. \tag{8}$$

For $t \to \infty$, one might expect $\tilde{\lambda}_{\langle \ln \rangle}$ to converge to $\tilde{\lambda}_{\ln\langle . \rangle}$. But for finite times, as discussed in Ref. [18], the quantum Lyapunov exponents Λ_Q are closer to $\tilde{\lambda}_{\ln\langle . \rangle}$ than to $\tilde{\lambda}_{\langle \ln \rangle}$, because Λ_Q is obtained from the logarithm of the fit. This closer proximity between Λ_Q and $\lambda_{\max}$ is confirmed for the Dicke model as well.

In Fig. 4, we compare the classical Lyapunov exponent $\tilde{\lambda}_{\langle \ln \rangle}$ (lower green horizontal line), the maximum classical Lyapunov exponent $\lambda_{\max}$ (black dotted line), the quantum Lyapunov exponents Λ_Q (red circles) for the fifty-one energy states, and the average over the quantum Lyapunov exponents (orange solid line surperposed by the line for $\lambda_{\max}$). The quantum exponents fluctuate due to the oscillations that modulate the exponential growth and to finite size effects; the standard deviation corresponds to the shaded area in the figure. Increasing the value of j would reduce this uncertainty. While $\tilde{\lambda}_{\langle \ln \rangle} = 0.112$, the maximum classical Lyapunov exponent, $\lambda_{\max} = 0.127$, coincides with the average value of the quantum Lyapunov exponent, $\bar{\Lambda}_Q = 0.126$, within its standard deviation $\sigma_\Lambda = 0.012$.

Discussion.— We showed that for the Dicke model in the chaotic region, the OTOC grows exponentially fast in time with a rate comparable to the classical Lyapunov exponent.

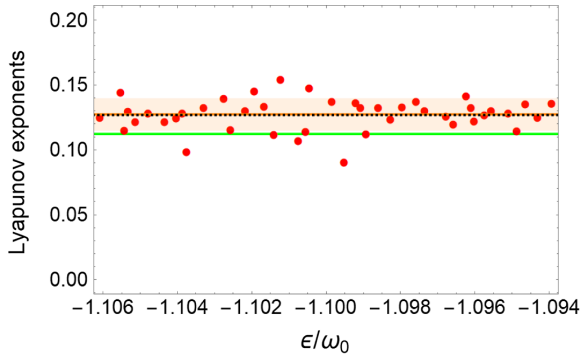

FIG. 4. Comparison between the classical Lyapunov exponent $\tilde{\lambda}_{\langle \ln \rangle}$ (lower green horizontal line), the maximum classical Lyapunov exponent $\lambda_{\max}$ (black dotted horizontal line), and the quantum Lyapunov exponents Λ_Q (red circles) for $C_n^{qp}(t)$ for fifty-one states of different energies around $\epsilon/\omega_0 \approx -1.1$. The solid orange line depicts the average value of Λ_Q and the shaded region represents the standard deviation around it.

These results confirm that the quantum-classical correspondence established by means of the OTOC is not exclusive to one-body systems, but is valid also for interacting systems with more than one degree of freedom. This work provides a proof-of-principle and should motivate similar studies in other interacting systems.

We stress that to clearly identify the quantum exponential growth and extract its rate, we need to have access to large system sizes. This was possible here, because we resorted to an efficient basis to construct the eigenstates.

The instrument of our analysis was the microcanonical OTOC [Eq. (3)] corresponding to the eigenstate expectation value of the commutator of two operators. Its use in stadium billiards [19] prevented the observation of the quantum exponential growth, which was only possible with the introduction of Gaussian states [20]. In our case, however, the eigenstates were excellent probe states for revealing the OTOC exponential growth. This is an important result for future studies of interacting systems, since the eigenstates are essential building blocks for thermal averages.

We thank L. Benet and T. Seligman for their useful comments. M. A. B. M., S. L. H., and J. G. H. acknowledge J. Dukelsky for fruitful discussions in the context of the Spanish Grant No. I-COOP2017:COOPB20289. P. S. is grateful to P. Cejnar for stimulating discussions. We acknowledge financial support from Mexican CONACyT Grant No. CB2015-01/255702, DGAPA-UNAM Grant No. IN109417 and RedTC. M. A. B. M. is a postdoctoral fellow of CONACyT. P. S. is supported by the Charles University Research Center Grant No. UNCE/SCI/013. L. F. S. is supported by the NSF Grant No. DMR-1603418.

[1] F. Haake, *Quantum Signatures of Chaos* (Springer-Verlag, Berlin, 1991).
[2] H.-J. Stöckmann, *Quantum Chaos: An Introduction* (Cambridge University Press, Cambridge, England, 2006).
[3] B. V. Chirikov, An example of chaotic eigenstates in a complex atom, Phys. Lett. **108A**, 68 (1985).
[4] V. V. Flambaum, A. A. Gribakina, G. F. Gribakin, and I. V. Ponomarev, Quantum chaos in many-body systems: What can we learn from the Ce atom?, Physica (Amsterdam) **131D**, 205 (1999).
[5] A. Peres, Chaotic evolution in quantum mechanics, Phys. Rev. E **53**, 4524 (1996).
[6] F. Borgonovi, F. M. Izrailev, and L. F. Santos, Exponentially fast dynamics in the Fock space of chaotic many-body systems, Phys. Rev. E **99**, 010101(R) (2019).
[7] R. A. Jalabert and H. M. Pastawski, Environment-Independent Decoherence Rate in Classically Chaotic Systems, Phys. Rev. Lett. **86**, 2490 (2001).
[8] F. M. Cucchietti, C. H. Lewenkopf, E. R. Mucciolo, H. M. Pastawski, and R. O. Vallejos, Measuring the lyapunov exponent using quantum mechanics, Phys. Rev. E **65**, 046209 (2002).
[9] T. Gorin, T. Prosen, T. H. Seligman, and M. Žnidarič, Dynamics of Loschmidt echoes and fidelity decay, Phys. Rep. **435**, 33 (2006).
[10] B. V. Fine, T. A. Elsayed, C. M. Kropf, and A. S. de Wijn, Absence of exponential sensitivity to small perturbations in nonintegrable systems of spins 1/2, Phys. Rev. E **89**, 012923 (2014).
[11] J. Maldacena and D. Stanford, Remarks on the Sachdev-Ye-Kitaev model, Phys. Rev. D **94**, 106002 (2016).
[12] J. Maldacena, S. H. Shenker, and D. Stanford, A bound on chaos, J. High Energy Phys. 08 (2016) 106.
[13] A. Larkin and Yu. N. Ovchinnikov, Zh. Eksp. Teor. Fiz. **55**, 2262 (1969) [Quasiclassical method in the theory of superconductivity, Sov. Phys. JETP **28**, 1200 (1969)].
[14] M. Gärttner, J. G. Bohnet, A. Safavi-Naini, M. L. Wall, J. J. Bollinger, and A. M. Rey, Measuring out-of-time-order correlations and multiple quantum spectra in a trapped-ion quantum magnet, Nat. Phys. **13**, 781 (2017).
[15] J. Li, R. Fan, H. Wang, B. Ye, B. Zeng, H. Zhai, X. Peng, and J. Du, Measuring Out-of-Time-Order Correlators on a Nuclear Magnetic Resonance Quantum Simulator, Phys. Rev. X **7**, 031011 (2017).
[16] K. X. Wei, C. Ramanathan, and P. Cappellaro, Exploring Localization in Nuclear Spin Chains, Phys. Rev. Lett. **120**, 070501 (2018).
[17] M. Niknam, L. F. Santos, and D. G. Cory, Sensitivity of quantum information to environment perturbations measured with the out-of-time-order correlation function, arXiv:1808.04375.
[18] E. B. Rozenbaum, S. Ganeshan, and V. Galitski, Lyapunov Exponent and Out-of-Time-Ordered Correlator's Growth Rate in a Chaotic System, Phys. Rev. Lett. **118**, 086801 (2017).
[19] K. Hashimoto, K. Murata, and R. Yoshii, Out-of-time-order correlators in quantum mechanics, J. High Energy Phys. 10 (2017) 138.
[20] E. B. Rozenbaum, S. Ganeshan, and V. Galitski, Universal level statistics of the out-of-time-ordered operator, arXiv:1801.10591.
[21] I. García-Mata, M. Saraceno, R. A. Jalabert, A. J. Roncaglia, and D. A. Wisniacki, Chaos signatures in the short and long time behavior of the out-of-time ordered correlator, arXiv:1806.04281.
[22] D. Bagrets, A. Altland, and A. Kamenev, Power-law out of time order correlation functions in the SYK model, Nucl. Phys. **B921**, 727 (2017).
[23] A. Bohrdt, C. B. Mendl, M. Endres, and M. Knap, Scrambling and thermalization in a diffusive quantum many-body system, New J. Phys. **19**, 063001 (2017).
[24] H. Shen, P. Zhang, R. Fan, and H. Zhai, Out-of-time-order correlation at a quantum phase transition, Phys. Rev. B **96**, 054503 (2017).
[25] T. A. Elsayed and B. V. Fine, Sensitivity to small perturbations in systems of large quantum spins, Phys. Scr. **T165**, 014011 (2015).
[26] M. Akila, D. Waltner, B. Gutkin, P. Braun, and T. Guhr, Semiclassical Identification of Periodic Orbits in a Quantum Many-Body System, Phys. Rev. Lett. **118**, 164101 (2017).

[27] E. Bianchi, L. Hackl, and N. Yokomizo, Linear growth of the entanglement entropy and the Kolmogorov-Sinai rate, J. High Energy Phys. 03 (2018) 25.
[28] T. Scaffidi and E. Altman, Semiclassical theory of many-body quantum chaos and its bound, arXiv:1711.04768.
[29] A. E. Tarkhov and B. V. Fine, Estimating ergodization time of a chaotic many-particle system from a time reversal of equilibrium noise, arXiv:1804.09732.
[30] J. Rammensee, J. D. Urbina, and K. Richter, Many-Body Quantum Interference and the Saturation of Out-of-Time-Order Correlators, Phys. Rev. Lett. **121**, 124101 (2018).
[31] R. H. Dicke, Coherence in spontaneous radiation processes, Phys. Rev. **93**, 99 (1954).
[32] B. M. Garraway, The dicke model in quantum optics: Dicke model revisited, Phil. Trans. R. Soc. A **369**, 1137 (2011).
[33] K. Hepp and E. H. Lieb, On the super-radiant phase transition for molecules in a quantized radiation field: The Dicke maser model, Ann. Phys. (N.Y.) **76**, 360 (1973); Y. K. Wang and F. T. Hioe, Phase transition in the Dicke model of super-radiance, Phys. Rev. A **7**, 831 (1973); H. J. Carmichael, C. W. Gardiner, and D. F. Walls, Higher order corrections to the Dicke super-radiant phase transition, Phys. Lett. **46A**, 47 (1973).
[34] K. Baumann, C. Guerlin, F. Brennecke, and T. Esslinger, Dicke quantum phase transition with a superfluid gas in an optical cavity, Nature (London) **464**, 1301 (2010).
[35] K. Baumann, R. Mottl, F. Brennecke, and T. Esslinger, Exploring Symmetry Breaking at the Dicke Quantum Phase Transition, Phys. Rev. Lett. **107**, 140402 (2011).
[36] H. Ritsch, P. Domokos, F. Brennecke, and T. Esslinger, Cold atoms in cavity-generated dynamical optical potentials, Rev. Mod. Phys. **85**, 553 (2013).
[37] M. P. Baden, K. J. Arnold, A. L. Grimsmo, S. Parkins, and M. D. Barrett, Realization of the Dicke Model using Cavity-Assisted Raman Transitions, Phys. Rev. Lett. **113**, 020408 (2014).
[38] J. Klinder, H. Keßler, M. Reza Bakhtiari, M. Thorwart, and A. Hemmerich, Observation of a super-radiant Mott Insulator in the Dicke-Hubbard Model, Phys. Rev. Lett. **115**, 230403 (2015).
[39] A. J. Kollár, A. T. Papageorge, V. D. Vaidya, Y. Guo, J. Keeling, and B. L. Lev, Supermode-density-wave-polariton condensation with a Bose-Einstein condensate in a multimode cavity, Nat. Commun. **8**, 14386 (2017).
[40] O. Castaños, R. López-Peña, J. G. Hirsch, and E. López-Moreno, Phase transitions and accidental degeneracy in nonlinear spin systems, Phys. Rev. B **72**, 012406 (2005).
[41] P. Pérez-Fernández, A. Relaño, J. M. Arias, P. Cejnar, J. Dukelsky, and J. E. García-Ramos, Excited-state phase transition and onset of chaos in quantum optical models, Phys. Rev. E **83**, 046208 (2011).
[42] T. Brandes, Excited-state quantum phase transitions in Dicke super-radiance models, Phys. Rev. E **88**, 032133 (2013).
[43] M. A. Bastarrachea-Magnani, S. Lerma-Hernández, and J. G. Hirsch, Comparative quantum and semiclassical analysis of atom-field systems. I. Density of states and excited-state quantum phase transitions, Phys. Rev. A **89**, 032101 (2014).
[44] J. Larson and E. K. Irish, Some remarks on super-radiant phase transitions in light-matter systems, J. Phys. A **50**, 174002 (2017).
[45] S. Schneider and G. J. Milburn, Entanglement in the steady state of a collective-angular-momentum (Dicke) model, Phys. Rev. A **65**, 042107 (2002); N. Lambert, C. Emary, and T. Brandes, Entanglement and the Phase Transition in Single-Mode super-radiance, Phys. Rev. Lett. **92**, 073602 (2004); M. Kloc, P. Stránský, and P. Cejnar, Quantum phases and entanglement properties of an extended Dicke model, Ann. Phys. (Amsterdam) **382**, 85 (2017).
[46] P. Pérez-Fernández, P. Cejnar, J. M. Arias, J. Dukelsky, J. E. García-Ramos, and A. Relaño, Quantum quench influenced by an excited-state phase transition, Phys. Rev. A **83**, 033802 (2011).
[47] A. Altland and F. Haake, Quantum Chaos and Effective Thermalization, Phys. Rev. Lett. **108**, 073601 (2012).
[48] S. Lerma-Hernández, J. Chávez-Carlos, M. A. Bastarrachea-Magnani, L. F. Santos, and J. G. Hirsch, Analytical description of the survival probability of coherent states in regular regimes, J. Phys. A **51**, 475302 (2018).
[49] M. Kloc, P. Stránský, and P. Cejnar, Quantum quench dynamics in Dicke super-radiance models, Phys. Rev. A **98**, 013836 (2018).
[50] C. H. Lewenkopf, M. C. Nemes, V. Marvulle, M. P. Pato, and W. F. Wreszinski, Level statistics transitions in the spin-boson model, Phys. Lett. A **155**, 113 (1991).
[51] C. Emary and T. Brandes, Quantum Chaos Triggered by Precursors of a Quantum Phase Transition: The Dicke Model, Phys. Rev. Lett. **90**, 044101 (2003); Chaos and the quantum phase transition in the Dicke model, Phys. Rev. E **67**, 066203 (2003).
[52] M. A. Bastarrachea-Magnani, S. Lerma-Hernández, and J. G. Hirsch, Comparative quantum and semiclassical analysis of atom-field systems. ii. Chaos and regularity, Phys. Rev. A **89**, 032102 (2014); M. A. Bastarrachea-Magnani, B. López del Carpio, S. Lerma-Hernández, and J. G. Hirsch, Chaos in the Dicke model: Quantum and semiclassical analysis, Phys. Scr. **90**, 068015 (2015); M. A. Bastarrachea-Magnani, B. López-del-Carpio, J. Chávez-Carlos, S. Lerma-Hernández, and J. G. Hirsch, Delocalization and quantum chaos in atom-field systems, Phys. Rev. E **93**, 022215 (2016).
[53] J. Chávez-Carlos, M. A. Bastarrachea-Magnani, S. Lerma-Hernández, and J. G. Hirsch, Classical chaos in atom-field systems, Phys. Rev. E **94**, 022209 (2016).
[54] O. Babelon, L. Cantini, and B. Douçot, A semi-classical study of the Jaynes-Cummings model, J. Stat. Mech. (2009) P07011.
[55] M. Kloc, P. Stránský, and P. Cejnar, Monodromy in Dicke super-radiance, J. Phys. A **50**, 315205 (2017).
[56] J. Cohn, A. Safavi-Naini, R. J. Lewis-Swan, J. G. Bohnet, M. Gärttner, K. A. Gilmore, J. E. Jordan, A. M. Rey, J. J. Bollinger, and J. K. Freericks, Bang-bang shortcut to adiabaticity in the Dicke model as realized in a penning trap experiment, New J. Phys. **20**, 055013 (2018).
[57] A. Safavi-Naini, R. J. Lewis-Swan, J. G. Bohnet, M. Garttner, K. A. Gilmore, J. E. Jordan, J. Cohn, J. K. Freericks, A. M. Rey, and J. J. Bollinger, Verification of a Many-Ion Simulator of the Dicke Model Through Slow Quenches Across a Phase Transition, Phys. Rev. Lett. **121**, 040503 (2018).

[58] Y. Alavirad and A. Lavasani, Scrambling in the Dicke model, arXiv:1808.02038.

[59] R. J. Lewis-Swan, A. Safavi-Naini, J. J. Bollinger, and A. M. Rey, Unifying fast scrambling, thermalization and entanglement through the measurement of FOTOCs in the Dicke model, arXiv:1808.07134.

[60] A. D. Ribeiro, M. A. M. de Aguiar, and A. F. R. de Toledo Piza, The semiclassical coherent state propagator for systems with spin, J. Phys. A **39**, 3085 (2006).

[61] L. Bakemeier, A. Alvermann, and H. Fehske, Dynamics of the Dicke model close to the classical limit, Phys. Rev. A **88**, 043835 (2013).

[62] M. A. Bastarrachea-Magnani and J. G. Hirsch, Efficient basis for the Dicke model: I. Theory and convergence in energy, Phys. Scr. **T160**, 014005 (2014); J. G. Hirsch and M. A. Bastarrachea-Magnani, Efficient basis for the Dicke model: II. Wave function convergence and excited states, Phys. Scr. **T160**, 014018 (2014).